AIMS Materials Science, 8(5): 716–738.
DOI:10.3934/matersci.2021043
Received: 06 July 2021
Accepted: 24 August 2021
Published: 23 September 2021

http://www.aimspress.com/journal/Materials

Research article

Numerical investigation of reinforced-concrete beam-column joints retrofitted using external superelastic shape memory alloy bars

Yamen Ibrahim Elbahy[1], Maged A. Youssef[1,*] and M. Meshaly[2,3]

[1] Civil and Environmental Engineering, Western University, London, Ontario, Canada, N6A 5B9
[2] Structural Engineering, Alexandria University, Alexandria, Egypt
[3] Construction & Building Engineering, Arab Academy for Science, Technology & Maritime Transport (AASTMT), Alexandria, Egypt

* **Correspondence:** Email: youssef@uwo.ca; Tel: +519-661-2111; Fax: 519-661-3779; Ext: 88661.

Abstract: The unique properties of Shape Memory Alloys (SMAs) have motivated researchers to use them as primary reinforcement in reinforced concrete (RC) structures. In this study, the applicability of using external unbonded SMA bars to retrofit RC beam-column joints (BCJs) is investigated. A three-dimensional finite element model, which simulates the suggested retrofitting technique, is first developed, and validated using ABAQUS software. The model is then further simplified and utilized to conduct a parametric study to investigate the behaviour of SMA retrofitted RC BCJs. Results of the parametric study are used to perform multiple linear regression analysis. Simple equations, which can be used to calculate the length and amount of SMA bars required to retrofit a RC BCJ, are then developed.

Keywords: reinforced concrete; shape memory alloys; beam-column joints; flexural behaviour; retrofit; finite element; ABAQUS; nonlinear behaviour

1. Introduction

Beam-column joints (BCJs) of reinforced concrete (RC) frames are seismically designed to satisfy the strong-column weak-beam concept, where severe inelastic deformations can occur in the

beam. Minimizing these inelastic deformations is needed to make seismically damaged structures repairable. In addition, one of the problems for existing RC structures, which were designed per pre-1970s standards, is the inadequate anchorage of the beam reinforcement in the BCJ area. Thus, these structures are assumed deficient under seismic loads. This highlights the urgent need to retrofit these structures to ensure safety of the occupants. Newly built structures may also need to be retrofitted to minimize the seismic residual deformations.

Different methods and techniques were suggested in the literature to improve the performance of RC BCJs. Bindhu et al. [1] proposed diagonal reinforcement bars to be used in the BCJ area to replace conventional stirrups. Yurdakul and Avsar [2] investigated repairing the damage of RC BCJs using carbon fiber-reinforced polymer (FRP) sheets. Chalioris and Bantilas [3] suggested improving the performance of RC BCJs by using X-bars in the BCJ area. Golias et al. [4] investigated using external X-shaped carbon-FRP ropes on both sides of the BCJ area. Golias et al. [5] suggested bonding carbon FRP sheets to both sides of the BCJ area.

Superelastic Shape Memory Alloys (SMAs) can undergo large strains and return to their undeformed shape upon unloading. The flagged-shape stress-strain hysteresis provides the damping ability. Also, SMAs have excellent fatigue properties and high corrosion resistance. All these unique properties make them potential candidate for retrofitting RC BCJs [6,7].

In this study, the applicability of retrofitting RC BCJs using external unbonded SMA bars is investigated. First, a finite element (FE) model is developed and validated using available experimental results. Then, a simplified model is suggested and validated using the FE model. An extensive parametric study is then carried out to investigate the behaviour of retrofitted RC BCJs. Results of the parametric study are used to develop equations that address the change in the behaviour of the retrofitted BCJs.

2. Proposed retrofitting technique

The proposed retrofitting technique is based on attaching external SMA bars to the RC BCJ. As shown in Figure 1, the bars are attached to the BCJ using external steel angles, which are attached to the BCJ using steel bolts. One angle is attached to the BCJ area, while the second angle is attached to the beam. Intermediate angles can be used for long SMA bars to make the bars follow the beam deflection.

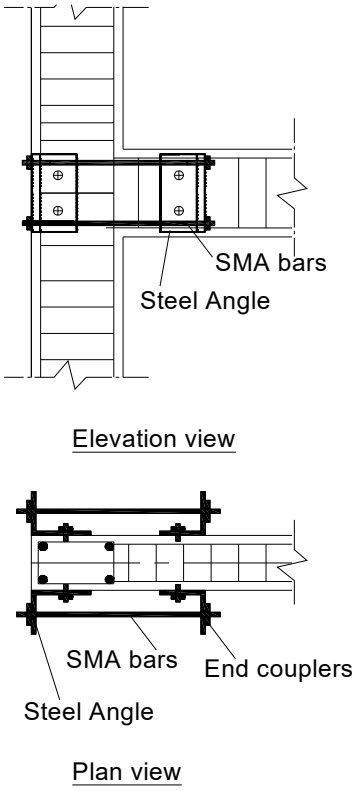

Figure 1. Proposed retrofitting technique.

3. Finite element simulation

Three-dimensional FE model was developed to investigate the behaviour of RC BCJs retrofitted using external SMA bars during loading and unloading stages. Analysis was performed using the commercial FE program ABAQUS Version 6.9 [8]. The modeling approach is presented in this section.

Concrete Damage Plasticity model, defined in the ABAQUS software, was used to model the concrete behaviour under both compressive and tensile loading. The model offers two main failure criteria: tensile cracking and compressive crushing of concrete. The uniaxial behaviour of the concrete under compression was based on the model developed by Scott et al. [9]. The tensile behaviour was based on the model developed by Stevens et al. [10] and modified by Youssef and Ghobarah [11]. Tension and compression damage parameters were defined in the concrete damage plasticity model to capture the degradation in strength and stiffness. The SMA material was represented using the model developed by Auricchio et al. [12]. The model was defined by a stress-strain curve and "breakpoint" stresses. This model requires, among other things, two moduli of elasticities, a plateau transformation strain, and five stress breakpoints. Elastic-plastic with isotropic hardening model was used to model the behaviour of steel elements.

Eight node reduced integration brick elements (C3D8R) were used to model the different elements, except for the stirrups which were modelled using 2-node 3-D truss elements (T3D2). C3D8R elements were chosen, as they offer balance between accuracy and computational efficiency.

4. Experimental validation

The developed 3-dimensional FE model was validated using available experimental results for BCJs that were internally reinforced with steel and SMA bars and for RC beams that were retrofitted using external steel and SMA bars.

4.1. Validation using BCJs

Results of the experimental work performed by Youssef et al. [13] were used to validate the accuracy of the developed FE model. Two large scale BCJs were constructed and tested under reversed-cyclic loading. The two BCJs were identical in dimensions and reinforcement details. However, they differed in the type of reinforcement in the plastic hinge region, which was regular steel bars for BCJ1 and superelastic SMA bars for BCJ2.

As shown in Figure 2, the beams of the two BCJs had a length of 1830 mm, 400 mm cross-section height, and 250 mm cross-section width. Amounts and arrangements of transverse reinforcement were also identical for the two beams. Stirrups were 10M spaced at 80 mm for the 800 mm length adjacent to the column and spaced at 120 mm elsewhere. The longitudinal top and bottom steel for the beam of BCJ1 was 2-20M. For BCJ2, 20.6 mm diameter superelastic SMAs bars were used to replace the top and bottom steel bars at the plastic hinge region. Steel couplers were used to connect the SMA bars to the 20M steel bars, which were located outside the plastic hinge region.

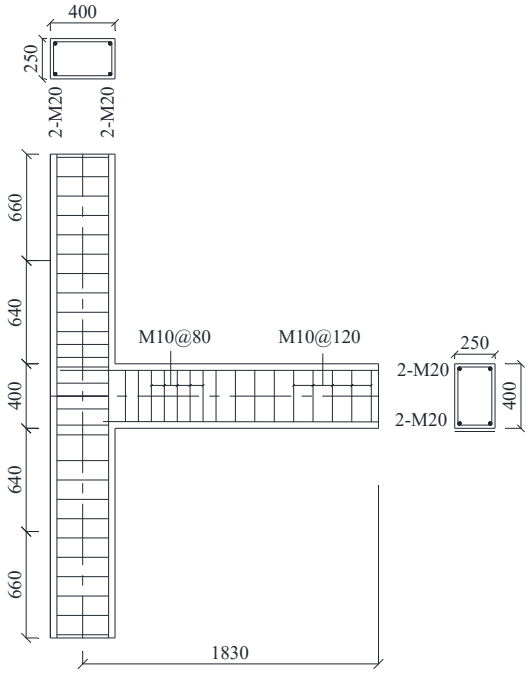

Figure 2. Details of the two BCJs tested by Youssef et al. Reprinted with permission from Ref. [13].

The average concrete compressive strength was 53.50 MPa for BCJ1 and 53.70 MPa for BCJ2. Average split cylinder tensile strength was 3.50 MPa for BCJ1 and 2.80 MPa for BCJ2. Steel

reinforcing bars of BCJ1 had yield strength of 520 MPa, ultimate strength of 653 MPa, and a modulus of elasticity of 198 GPa. Steel reinforcing bars of BCJ2 had yield strength of 450 MPa, ultimate strength of 650 MPa, and a modulus of elasticity of 193 GPa. Stirrups had a yield strength of 422 MPa and ultimate strength of 682 MPa.

Youssef et al. [13] determined the mechanical properties of the superelastic SMA bars by experimentally testing them under cyclic loading. It was reported that the SMA bars critical stress was 401 MPa at a critical strain of 0.75%. The modulus of elasticity was evaluated as 62.5 GPa. The residual strain was determined as 0.73%, when the SMA bar was loaded up to 6.0% strain.

Mesh sensitivity analysis was first performed. Five different element sizes (46.88, 39.07, 31.25, 25.40 and 19.05 mm) were considered. As shown in Figure 3, element size of 25.4 mm gave good results for the two BCJs and further refinement of the mesh did not noticeably change the behaviour. Experimental results were plotted versus the analytical results for the two BCJs in Figure 4, good agreement between the experimental and analytical results can be observed for the two BCJs.

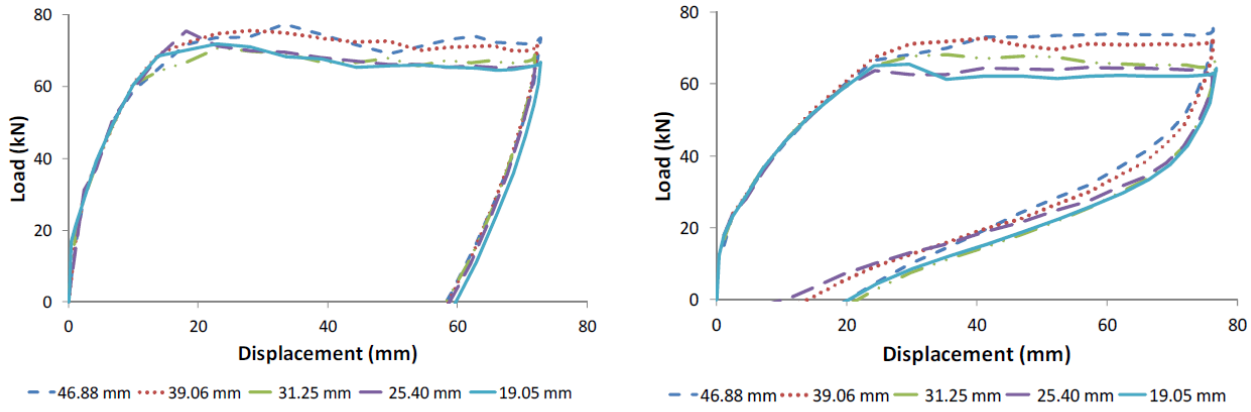

Figure 3. Mesh sensitivity analysis for the FE analysis: (a) BCJ1, and (b) BCJ2.

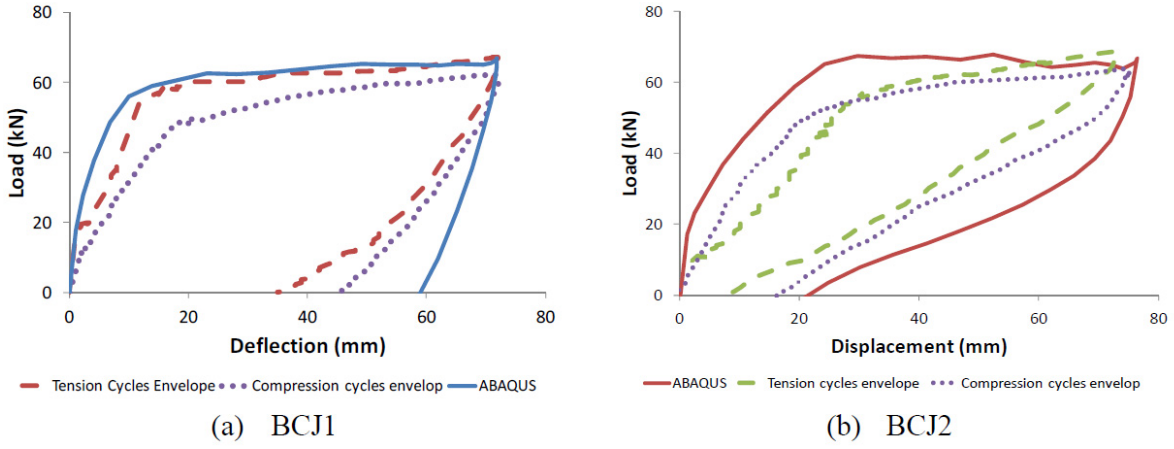

Figure 4. Experimental vs. FE load-displacement results (a) BCJ1, and (b) BCJ2.

4.2. *Validation using externally reinforced beams*

The work done by Saiidi et al. [14] was used to validate the model accuracy in predicting the behaviour of RC beams externally reinforced with steel or SMA bars. Saiidi et al. [14] tested eight RC beams under quasi-static loading. The eight beams are different in the type and amount of reinforcement at the mid-span as summarized in Table 1. Four beams are reinforced with SMA bars at mid-span, while the other four are reinforced with conventional steel bars.

Table 1. Properties of the beams tested.

Specimen	Mid-span reinforcement	ε_y (mm/mm)	f_y (MPa)	E_y (MPa)
BNL1	1 Φ 6.40 mm	0.013	400	34078
BNL2	2 Φ 6.40 mm	0.013	400	34078
BNH1	1 Φ 9.50 mm	0.013	510	39245
BNH2	2 Φ 9.50 mm	0.013	510	39245
BSL1	1 Φ 9.53 mm	0.0021	440	209524
BSL2	2 Φ 9.53 mm	0.0021	440	209524
BSH1	1 Φ 12.70 mm	0.0009	420	466667
BSH2	2 Φ 12.70 mm	0.0009	420	466667

The beams are 1530 mm long. They had cross-sectional dimensions of 127 × 152 mm at mid-span and 127 × 305 mm at the ends, Figure 5. The beams were tested under two-point symmetric loads that were placed 152 mm apart. The reinforcement at mid-span was attached to the beam using external angles. The internal reinforcement was cut at the mid-span section to ensure that the behaviour is controlled by the external reinforcement.

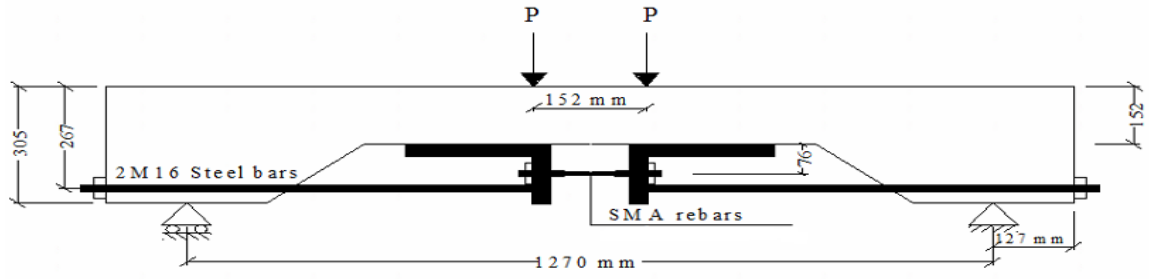

Figure 5. Beams dimensions and test setup.

Mesh sensitivity analysis was performed to determine the appropriate element size. As shown in Figure 6, four element sizes were used in the analysis. It was found that reducing the element size beyond 25.4 mm had negligible effect on the predicted results. Results of the analysis are plotted in Figure 7 for the SMA RC beams and in Figure 8 for the steel RC beams. As shown in the figures, good agreement between the experimental and analytical results is observed for both steel and SMA RC beams.

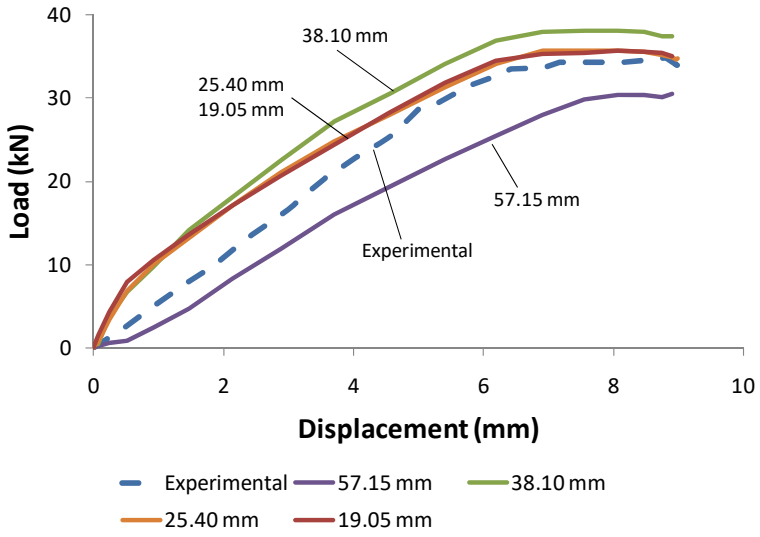

Figure 6. Mesh sensitivity analysis for beam BNH1.

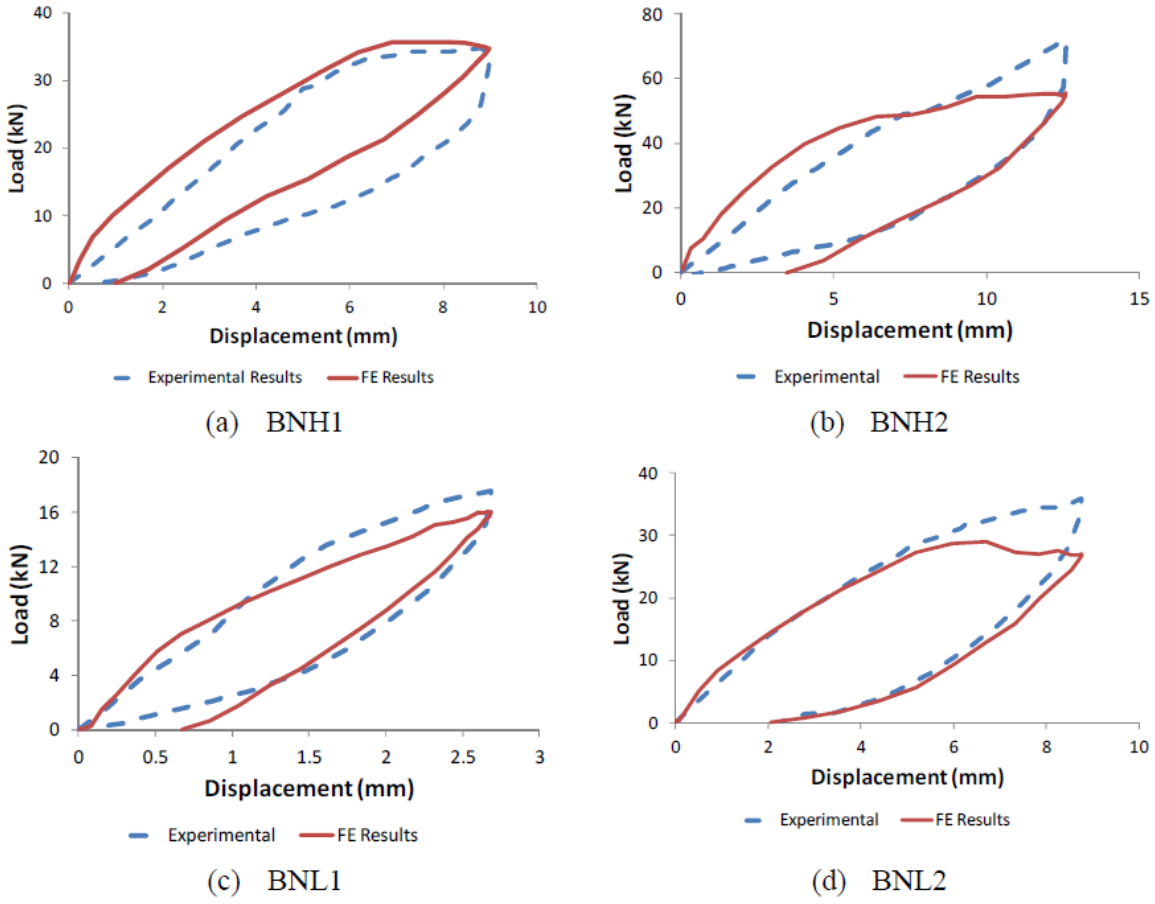

Figure 7. Experimental vs. analytical results for SMA RC beams: (a) BNH1, (b) BNH2, (c) BNL1, and (d) BNL2.

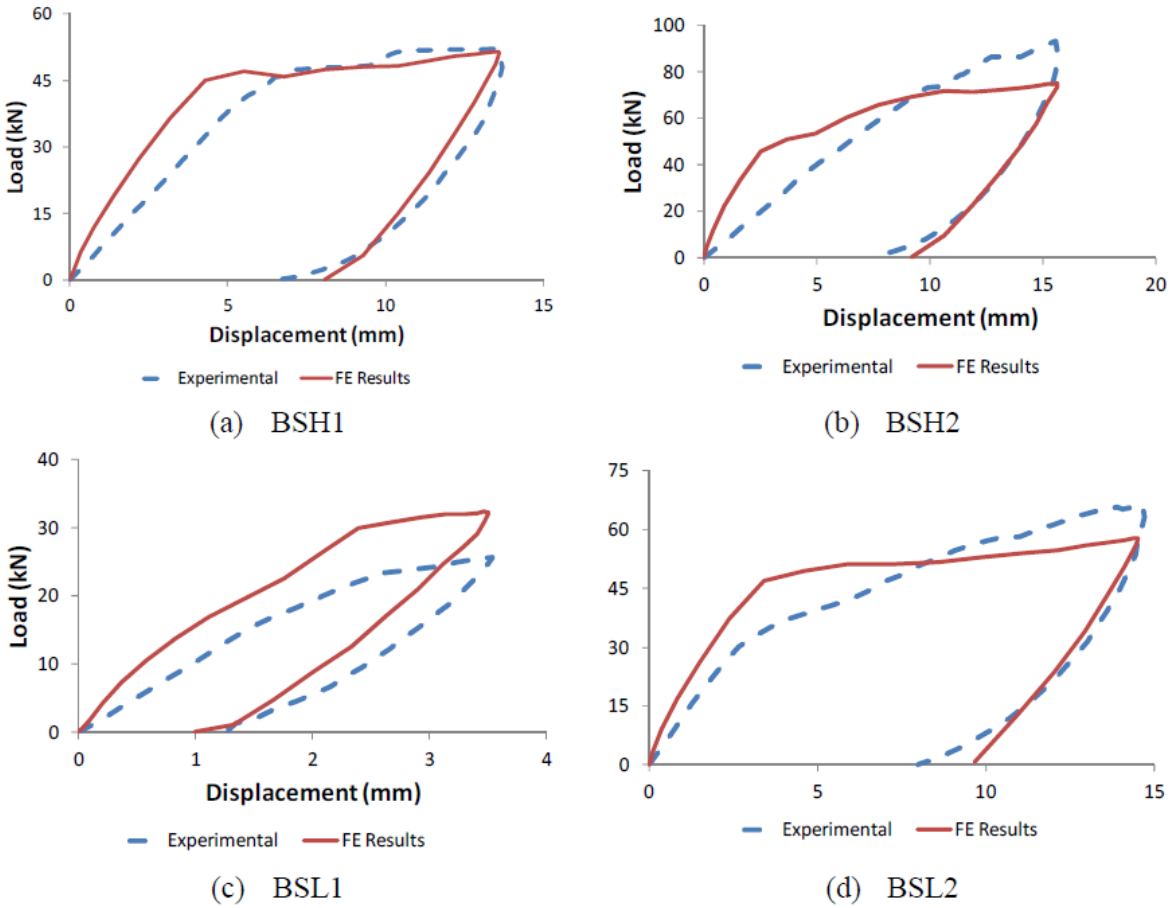

Figure 8. Experimental vs. analytical results for steel RC beams; (a) BSH1; (b) BSH2; (c) BSL1; and (d) BSL2.

5. Retrofitted BCJ

A RC BCJ was assumed for the analysis in this section, Figure 9. The beam of the BCJ had a cross-section of 250 × 400 mm and a span of 1830 mm. The column had similar cross-section and was 1200 mm in height. The loading plates had dimensions equal to 250 × 400 × 100. The external angles had dimensions of 90 × 90 × 20 mm and were attached to the BCJ using 8 bolts. The bolts were assumed to be 71 mm in length and 12.7 mm in diameter. The external SMA bars were attached to the external angles using end couplers. The added external SMA bars were equal to the internal steel reinforcement.

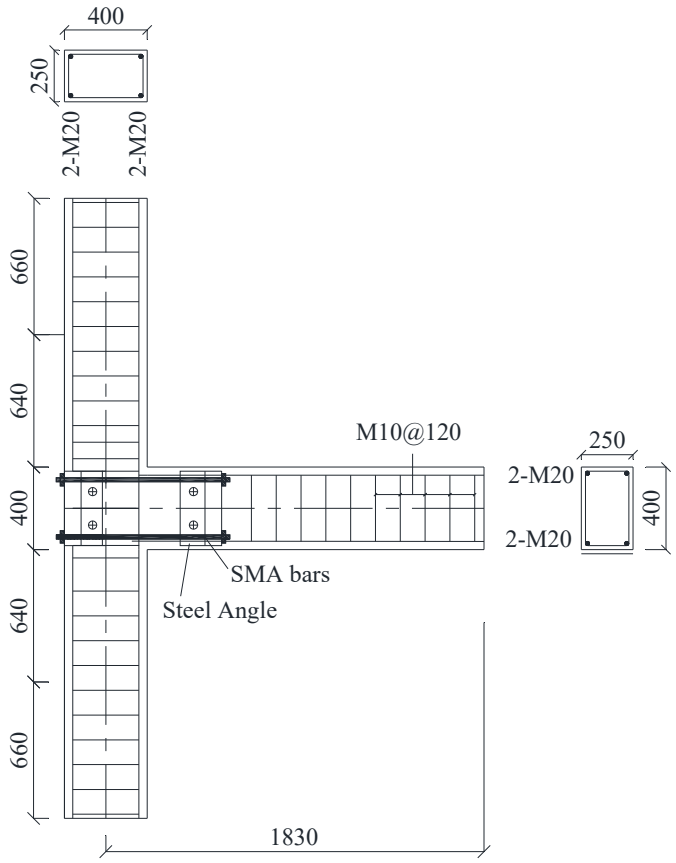

Figure 9. Sketch of the retrofitted BCJ.

5.1. Model

The FE model was assembled of separate parts as shown in Figure 10. These parts include the RC BCJ, loading plates, external angles, external SMA bars, bolts, internal steel bars, and stirrups. Different contact models were used to model the interaction between the different parts. The contact between the top/bottom rigid steel plates and the RC column was a tie contact type. Tie contact was also used to model the assumed perfect bond between the concrete and the internal longitudinal bars. Embedded region contact was used to model the perfect bond between the steel stirrups and the concrete. Kinematic surface-to-surface contact was used to define the interaction between the BCJ and the external angles, as well as the angles and the bolts. Bolts were assumed to have perfect bond with concrete. A rigid body, located at the beam tip, was used to apply the load.

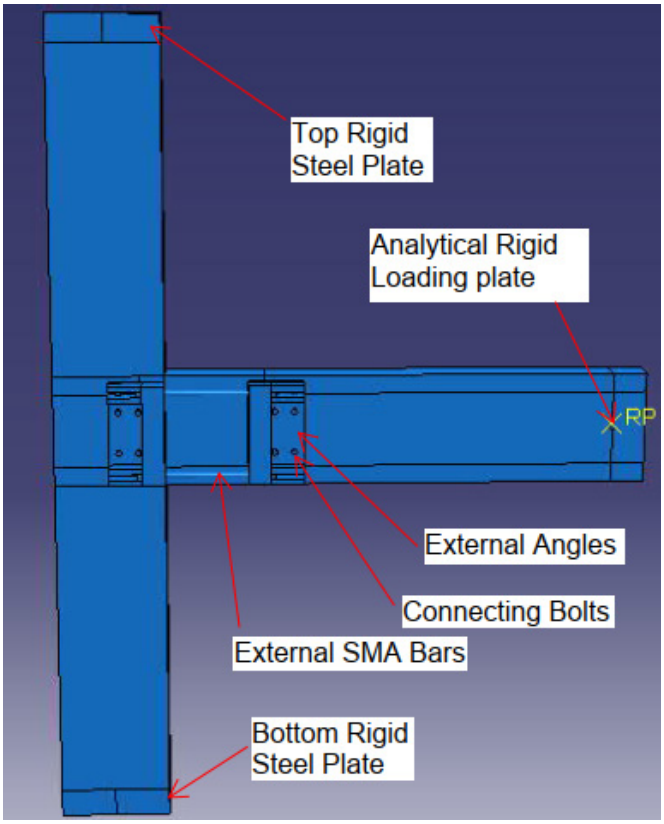

Figure 10. Parts of the Modeled BCJ.

Two boundary conditions were used in the developed FE model. The bottom end of the column was restrained in all three directions, while the top end was restrained only in two directions. It was allowed to move vertically to transfer the compressive column force.

Loading of the BCJ was performed in three stages. First stage was applying compressive stress at the top of the column. The compressive pressure was applied to the rigid steel plate, which ensures proper distribution of the pressure and eliminates localized distortions in the concrete. Second stage was to apply monotonic displacement using the rigid body near the tip of the beam. After reaching the predefined maximum displacement, unloading started in a similar fashion to the beam loading stage.

Mesh sensitivity analysis was performed to eliminate effects of the elements size on the analysis results. Element size of 25.40 mm was found to be the most appropriate in terms of accuracy and analysis time. Figure 11 shows the meshed FE model of the retrofitted BCJ.

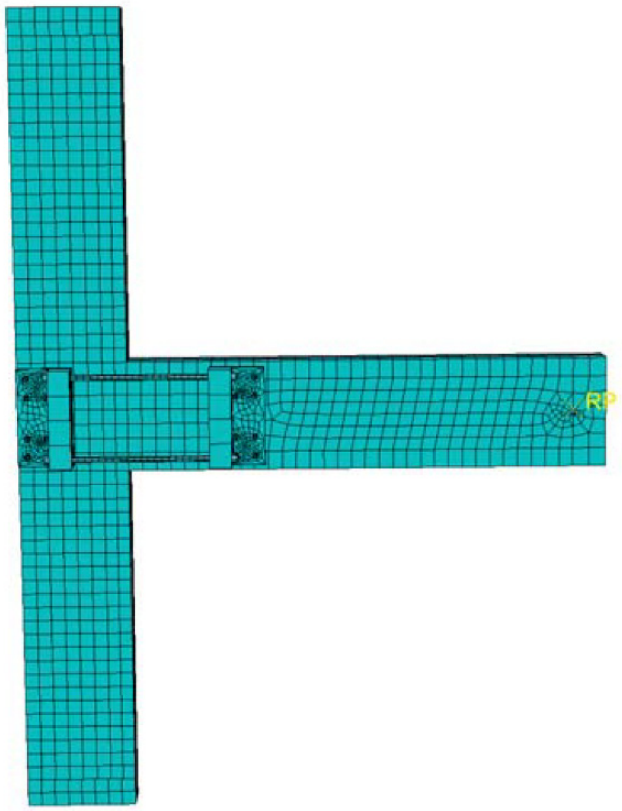

Figure 11. FE Model of the retrofitted BCJ.

5.2. Results of the retrofitted beam

Figure 12 shows the load-displacement relationship of the retrofitted and the original beams. Retrofitting increased the maximum moment capacity from 70 to 85 kN·m, did not affect the initial stiffness, reduced theresidual displacement from 72 to 60 mm, and increased the amount of dissipated energy. It is clear from the figure that adding external SMA bars reduced the amount of residual displacement by 17%. This small effect is attributed to the low modulus of elasticity for the SMA bars. Thus, attaching a small to moderate ratio of SMA bars is expected to improve the strength of the BCJ, but it is not expected to reduce the residual deformations. To further benefit from the added SMA bars, it is proposed to cut the internal steel bars of the beam at the face of the column and replace them with the external SMA bars. This ensures that the BCJ behaviour is governed by the external SMA bars rather than the internal steel bars.

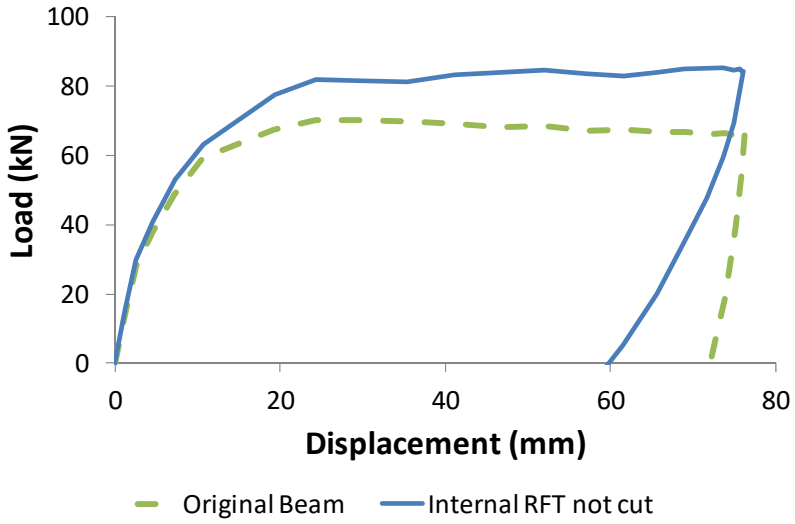

Figure 12. FE load-displacement relationship for the original BCJ vs. the retrofitted BCJ.

FE analysis was performed again for the BCJ assuming cutting the internal steel reinforcement. Results are illustrated in Figure 13. As shown in the figure, significant reduction in the residual displacement (98%) was observed. On the other hand, the total moment capacity of the beam was reduced by 31%. Initial stiffness of the beam was also significantly reduced. These disadvantages can be overcome by increasing the amount of the external SMA bars as investigated in the following sections.

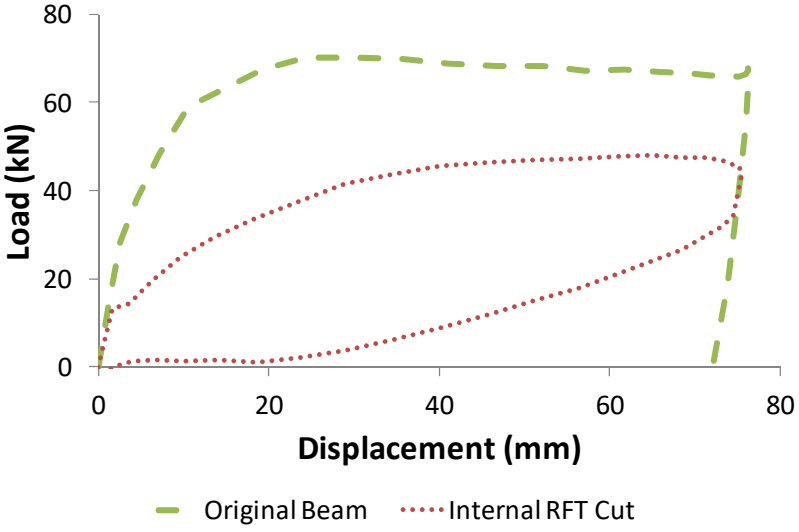

Figure 13. FE load-displacement relationship for the original BCJ vs. the retrofitted BCJ with internal steel bars are cut.

Typical cracking pattern of the retrofitted RC BCJ is given in Figure 14. The cracking pattern is presented in terms of the damage percentage for the elements. As expected, most of the cracking

happened to the BCJ near the interface between the column and the beam and at the elements connected to the retrofit bolts. For this case, the average damage of the elements reached 75%.

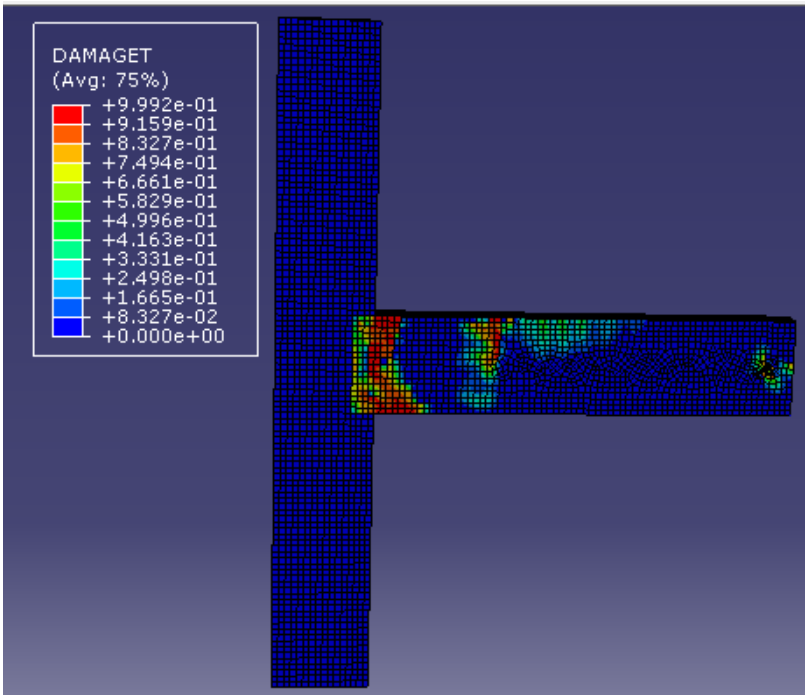

Figure 14. Typical cracking pattern of the retrofitted BCJ.

6. Simplified model

Modelling the retrofitted BCJ using ABAQUS is a complex process. Thus, a simplified model for the retrofitted BCJ is proposed in this section. The simplified model was developed using SeismoStruct software v.6 [15]. The special technique used to model the connection include: (i) modelling the SMA bars using inelastic truss elements; (ii) modelling the superelastic behaviour of the SMA bars using the uniaxial material model proposed by Auricchio and Sacco [16]; (iii) modelling the beam and column using displacement based inelastic frame elements; and (iv) modelling the external angles using rigid arms.

Figure 15 shows frame elements modeling the beam and the column. Two rigid arms are connected to the beam near the face of the column to represent the angle in the BCJ area. Another two rigid arms are connected to the beam at a distance equal to the length of the required SMA bars. The SMA bars are connected between the rigid arms and are modelled using truss elements. The reinforcement in the beam element is cut in between the rigid arms.

To validate the assumed simplified model, a comparison between the load-displacement results of the simplified model, developed using SeismoStruct software, and the actual model, developed using ABAQUS, is shown in Figure 16. Very good agreement between the two results was achieved.

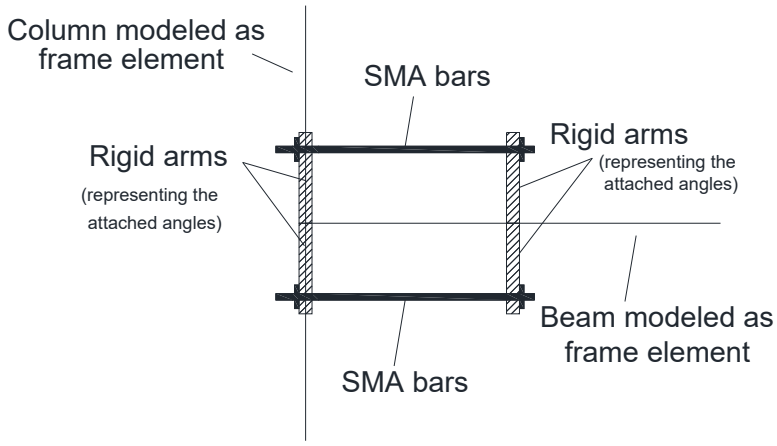

Figure 15. Sketch of the simplified model.

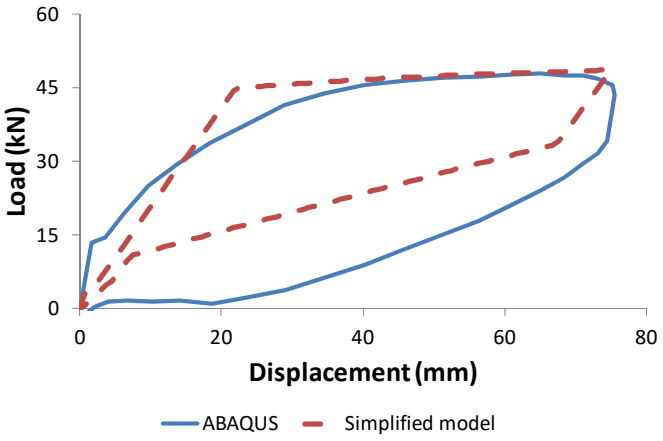

Figure 16. Load-displacement results of the ABAQUS model vs. the simplified SeismoStruct model.

7. Parametric study

A parametric study is carried out in this section to investigate the behaviour of RC BCJs retrofitted using external SMA bars. The analysis was performed using the developed simplified model. One cycle of loading-unloading was used for each case in the parametric study analysis. Three different parameters were investigated in this study: (i) ratio between the added external SMA reinforcement to the amount of internal steel reinforcement in the beam (A_{SMA}/A_s); (ii) ratio between the length of the used SMA bars to the length of the beam (L_{SMA}/L); and (iii) drift ratio (δ_{max}/L).

The parametric study was performed on BCJs with geometrical dimensions similar to that presented in the FE Simulation section. The beams were loaded/unloaded using a point load applied at the cantilever tip. For each of the studied parameters, the parameter under investigation is varied within the desired range while keeping all other parameters constant during the analysis. Four different outputs are used to compare the results of the parametric study. These outputs are: (i) ratio between the residual displacement upon complete unloading (δ_r) and the maximum displacement applied to the beam tip (δ_{max}); (ii) ratio between the maximum moment capacity of the retrofitted

BCJ (M_{rt}) to the moment capacity of the original BCJ (M_{org}); (iii) ratio between the secant stiffness of the retrofitted BCJ (ST_{rt}) to the secant stiffness of the original BCJ (ST_{org}); and (iv) amount of dissipated energy by the retrofitted BCJ (EN_{rt}) to amount of dissipated energy by the original BCJ (EN_{org}). Internal steel reinforcement is assumed to be cut in all studied BCJs.

8. Results and discussions

8.1. A_{SMAs}/A_s parameter

Ten different A_{SMA}/A_s ratios were used in the analysis. These ratios are: A_{SMA}/A_s = 0.5, 1.0, 1.5, 2.0, 2.5, 3.0, 3.5, 4.0, 4.5, and 5.0. The analysis was performed for nine SMA lengths ranging between 0.125L to 1.0L. Results of the analysis are plotted in Figure 17.

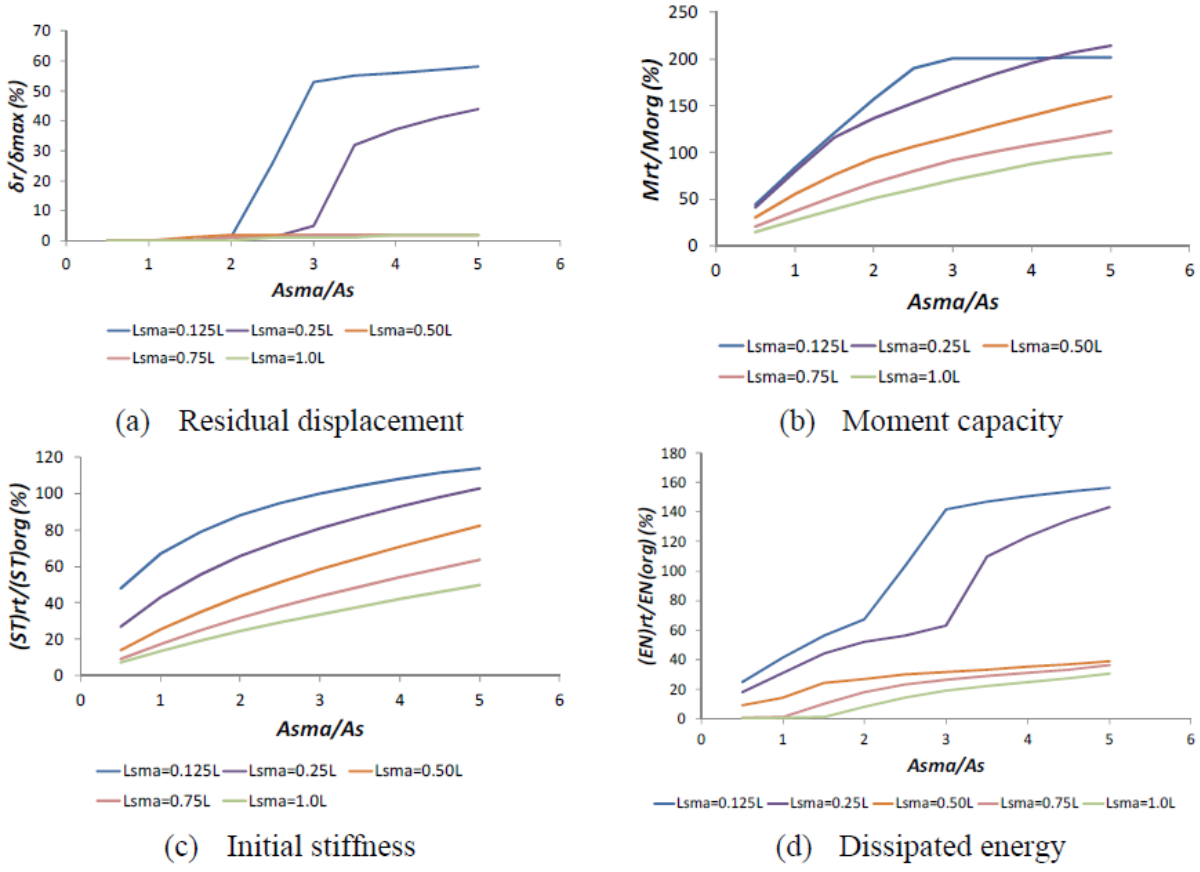

Figure 17. Effect of varying the A_{SMA}/A_s ratio on: (a) residual displacement; (b) moment capacity; (c) initial stiffness; and (d) dissipated energy.

Residual displacement at complete unloading from the failure point was found to be negligible at small A_{SMA}/A_s ratios. As A_{SMA}/A_s ratio increased from 2.0 to 3.0, δ_r/δ_{max} ratio increased from 1.0% to almost 53% in case of L_{SMA}/L = 0.125. For L_{SMA}/L = 0.25, an increase in δ_r/δ_{max} ratio of 30% occurred when A_{SMA}/A_s ratio increased from 3.0 to 3.5. This increase in the residual displacements

can be attributed to the change happening in the cross-section status from an under-reinforced section to an over-reinforced section. For L_{SMA}/L = 0.50 and higher, δ_r/δ_{max} ratio remained constant at 2.0%.

The moment capacity of the BCJ was found to increase with the increase in the A_{SMA}/A_s ratio. The rate of increase significantly varies with the L_{SMA}/L ratio. Higher rate of increase in case of L_{SMA}/L = 0.125 and 0.25 was observed. For case of L_{SMA}/L =0.125, the increase of M_{rt}/M_{org} ratio was almost 200%. Further increase in the A_{SMA}/A_s ratio did not increase the moment capacity. This means that the failure in the BCJ was governed by the concrete crushing rather than the yielding of the SMA bars.

The initial stiffness of the BCJ was found to increase with the increase in the A_{SMA}/A_s ratio for all L_{SMA}/L ratios. However, the rate and amount of increase significantly varies with the length of the SMA bars. It can also be noted that the initial stiffness was smaller than that of the original BCJ except for small L_{SMA}/L ratios (0.125 and 0.25).

Amount of dissipated energy was found to slightly increase with the increase in the A_{SMA}/A_s ratio. For case of L_{SMA}/L = 0.125 and 0.25, there was a sudden change in the amounts of dissipated energy at A_{SMA}/A_s values ranging between 2.0 and 3.5. This sudden change was attributed to the mode of failure of the cross-section, which changed from SMA bars yielding to concrete crushing.

8.2. L_{SMA}/L parameter

SMA bars length was represented by the ratio (L_{SMA}/L), which is the ratio between the length of the used SMA bars to the total length of the beam. Nine different SMA bar lengths were assumed in the analysis. These lengths are: L_{SMA}/L = 0.125, 0.167, 0.20, 0.25, 0.333, 0.50, 0.667, 0.75, and 1.0. Each length was analyzed at different A_{SMA}/A_s ratios (A_{SMA}/A_s = 0.50, 1.0, 1.5, 2.0, 2.5, 3.0, 3.5, 4.0, 4.5, and 5.0). Results of the analysis are presented in Figure 18.

Increasing the length of the SMA bars resulted in significant reduction in the residual deformations. The ratio δ_r/δ_{max} reduced from 70% to 3%, when L_{SMA}/L increased from 0.125 to 0.333 for A_{SMA}/A_s = 3.0. Considering A_{SMA}/A_s = 1.0 and 2.0, almost no change in the residual deformations was noted. The moment capacity of the retrofitted BCJs was found to decrease with the increase of L_{SMA}/L. The reduction occurred for all ratios of A_{SMA}/A_s. However, the rate and amount of reduction varied with A_{SMA}/A_s values. For example, the moment capacity was reduced from 220% to almost 100% in case of A_{SMA}/A_s = 5.0, while it was reduced from 80% to 30% in case of A_{SMA}/A_s = 1.0.

The initial stiffness of the retrofitted BCJ was found to decrease with the increase of L_{SMA}/L. Similar behaviour was observed for all values of the A_{SMA}/A_s. ST_{rt}/ST_{org} was reduced from 120% to 50% when L_{SMA}/L increased from 0.125 to 1.0 for the case of A_{SMA}/A_s = 5.0 and from 70% to 10% for the case of A_{SMA}/A_s = 1.0. Amount of dissipated energy was found to significantly decrease with the increase in L_{SMA}/L. EN_{rt}/EN_{org} was decreased from 160% to 30% when the L_{SMA}/L ratio increased from 0.125 to 1.0 for the case of A_{SMA}/A_s = 5.0, and from 40% to 0% for the case of A_{SMA}/A_s = 1.0.

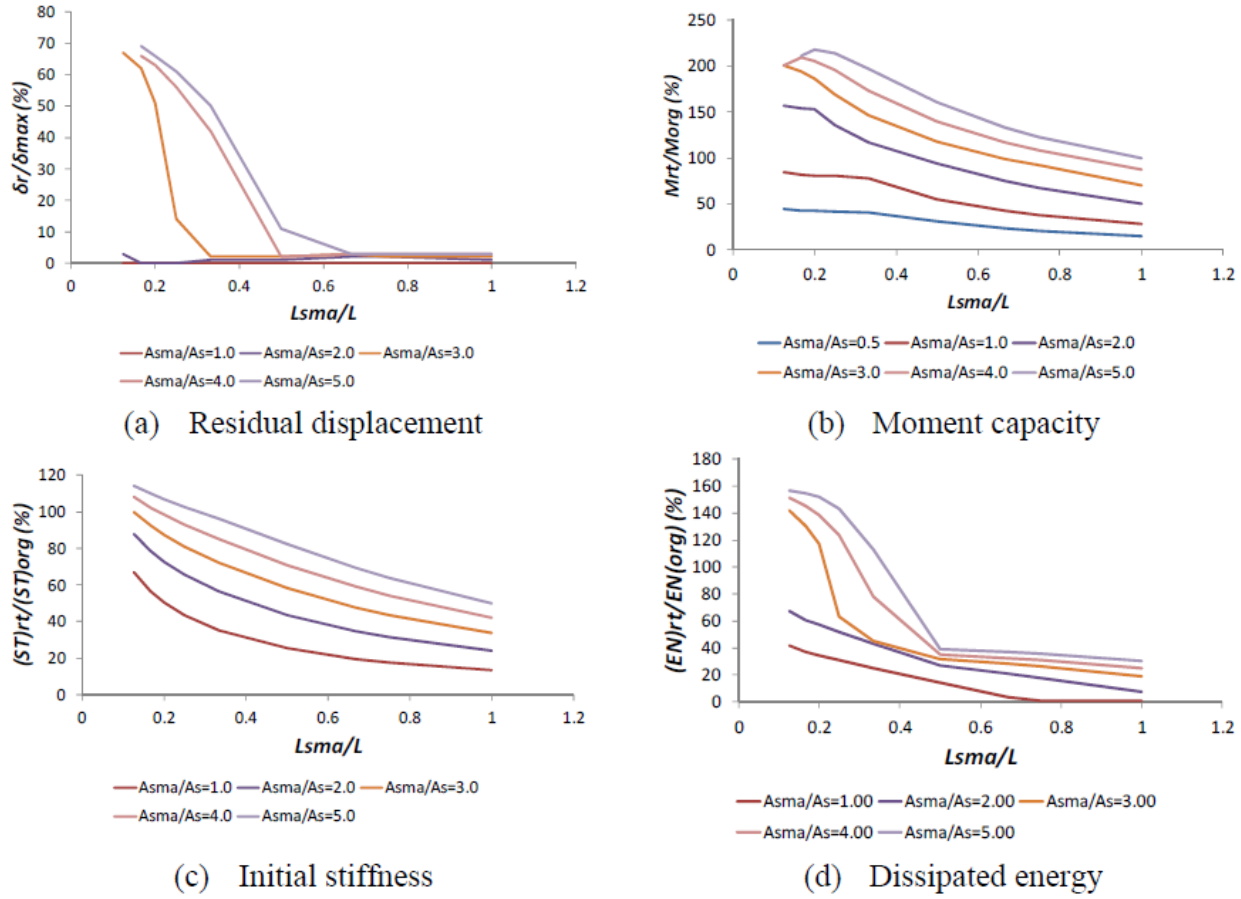

Figure 18. Effect of varying the L_{SMA}/L ratio on: (a) residual displacement, (b) moment capacity, (c) initial stiffness, and (d) dissipated energy.

8.3. Drift ratio parameter

The effect of varying the drift ratio on the behaviour of RC BCJs retrofitted using external SMA bars was investigated in this section. The analysis was performed for different values of A_{SMA}/A_s at different drift ratios. The drift ratio was represented by the ratio between the beam-tip maximum deflection (δ_{max}) to the length of the beam (L). The analysis was performed for three different drift ratios. Figure 19 illustrates the results of the analysis.

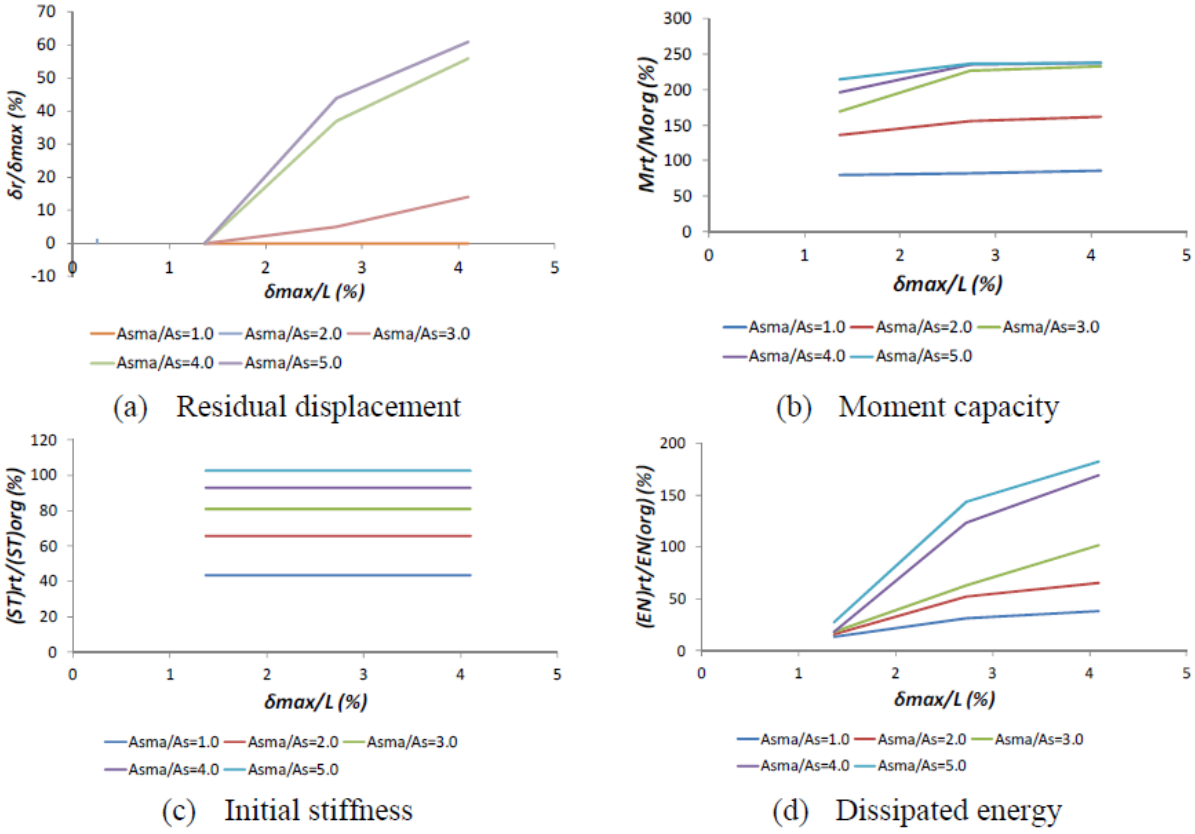

Figure 19. Effect of varying the drift ratio on: (a) residual displacement, (b) moment capacity, (c) initial stiffness, and (d) dissipated energy.

The residual displacements were found to significantly increase (60%) with the increase in the drift ratio for A_{SMA}/A_s = 4.0 and 5.0. The increase was smaller (15%) in case of A_{SMA}/A_s = 3.0. For cases with low A_{SMA}/A_s (i.e., 1.0 and 2.0), no change in the amount of residual displacement was observed. Slight increase in the BCJ moment capacity occurred with the increase in the drift ratio. This slight increase was attributed to the strain hardening of the SMA bars. The initial stiffness of the BCJ was found to be independent of the drift ratio. Amount of dissipated energy increased with the increase in the drift ratio. The rate and amount of increase of the dissipated energy was dependent on A_{SMA}/A_s ratio. It was observed that the higher the A_{SMA}/A_s ratio, the larger the amount of dissipated energy.

9. Choice of SMA bars length

Results of the parametric study were arranged in a database format. Multiple linear regression was then used to determine the relationships between the inputs and outputs of the study. Numerous models based on different transformations (i.e., linear, quadratic, and logarithmic) were first tried. The best models that relate the parametric study inputs to outputs were then chosen.

The used regression analysis methodology is called backward elimination stepwise regression [17]. In this technique, all explanatory variables (inputs) are included in the model at the

beginning. Then, the non-significant variables are eliminated one at a time in each trial. At the end of the analysis, the reported remaining variables are only the statistically significant ones.

A total of 524 data sets were used in establishing the statistical models. All inputs and outputs are kept dimensionless. The inputs are: (i) internal reinforcement status (bars are cut or not); (ii) A_{SMA}/A_s ratio; (iii) L_{SMA}/L ratio; and (iv) drift ratio. The outputs of the parametric study are: δ_r/δ_{max}, M_{rt}/M_{org}, ST_{rt}/ST_{org}, and EN_{rt}/EN_{org}. Descriptive statistics of the used data are presented in Table 2.

Correlation analysis was first used with the data to determine the correlation between each pair of variables and to note the highly correlated ones. The correlation matrix is determined using the STATA software V.12 and is shown in Table 3. Tables 4–7 present the final regression models for the five outputs. All coefficients reported in these tables are statistically significant with 95% confidence level, as the associated p-values are less than 0.05. Measures of model goodness-of-fit (represented by *R-squared*, *Adj R-squared,* and *Root Mean Square Error-MSE*) are also reported in each table. All models are considered to provide very good fit as their *R-squared* values range from 0.72 to 0.98. Furthermore, the values of MSE range from 0.16 to 15.0 confirming also a very good model fit [18]. Eqs 1–4 represent the summary of the final statistical models for the four outputs.

$$(\delta_r/\delta_{max}) = -43.8554 \times (\text{Reinforcement status}) - 3.05824 \times (\delta_{max}/L)^2 + 24.97149 \times (\delta_{max}/L) + 48.73263 \times (L_{SMA}/L)^2 - 63.5142 \times (L_{SMA}/L) + 0.299076 \times (A_{SMA}/A_s)^2 + 23.85597 \quad (1)$$

$$\ln(M_{rt}/M_{org}) = 0.351534 \times (\delta_{max}/L) - 0.03753 \times (\delta_{max}/L)^2 - 0.70269 \times (L_{SMA}/L)^2 + 0.736527 \times \ln(A_{SMA}/A_s) + 3.829082 \quad (2)$$

$$(ST_{rt}/ST_{org}) = 63.86686 \times (L_{SMA}/L) + 24.46517 \times (L_{SMA}/L)^2 - 1.92955 \times (A_{SMA}/A_s)^2 + 56.02788 \quad (3)$$

$$\ln(EN_{rt}/EN_{org}) = 2.085338 \times (\delta_{max}/L) - 0.25739 \times (\delta_{max}/L)^2 - 4.36291 \times (L_{SMA}/L) + 0.985633 \times (L_{SMA}/L)^2 + 1.194 \times \ln(A_{SMA}/A_s) + 0.415448 \quad (4)$$

A steel RC BCJ to be retrofitted with the suggested retrofitting technique was assumed to illustrate the use of the presented equations. Examining the behaviour of the BCJ at δ_{max}/L = 2.0%, after retrofitting using external SMA bars (L_{SMA}/L = 20% and A_{SMA}/A_s = 150%), revealed that the residual displacement at complete unloading reduces to only 7% of the maximum applied displacement, the moment capacity improves by 5%, the initial stiffness reduces to 66% of its original value, and the amount of dissipated energy reduces to 25% of its original value.

Table 2. Descriptive statistics of the used data.

Variable	Obs	Mean	Std. Dev.	Min	Max
RFT status	524	0.51	0.50	0	1
δ_{max}/L	524	2.70	1.11	1.37	4.10
L_{SMA}/L	524	0.44	0.28	0.13	1
A_{SMA}/A_s	524	2.74	1.44	0.5	5
δ_r/δ_{max}	524	31.07	28.61	−1.42 E−13	83
M_{rt}/M_{org}	524	181.42	67.76	14.77	354.78
ST_{rt}/ST_{org}	524	97.61	44.57	7.20	180.74
EN_{rt}/EN_{org}	524	100.82	69.90	0.03	260.50

Table 3. Correlation coefficients between all variables.

	RFT status	δ_{max}/L	L_{SMAs}/L	A_{SMA}/A_s	δ_r/δ_{max}	M_{rt}/M_{org}	ST_{rt}/ST_{org}	EN_{rt}/EN_{org}
RFT status	1							
δ_{max}/L	0.02	1						
L_{SMA}/L	0.03	−0.01	1					
A_{SMA}/A_s	0.00	−0.01	−0.01	1				
δ_r/δ_{max}	−0.76	0.31	−0.14	0.07	1			
M_{rt}/M_{org}	−0.48	0.21	−0.22	0.66	0.47	1		
ST_{rt}/ST_{org}	−0.83	−0.02	−0.16	0.40	0.74	0.79	1	
EN_{rt}/EN_{org}	−0.75	0.35	−0.22	0.30	0.90	0.71	0.85	1

Table 4. Regression model for δ_r/δ_{max}.

Source	SS	df	MS	Goodness-of-fit	δ_r/δ_{max}	Coef.	Std. Err.	t	P > t	(95% Conf. Interval)	
Model	311799.6	6	51966.6	Number of obs = 524	RFT status	−43.8554	1.312181	−33.42	0	−46.4333	−41.2775
Residual	116419.6	517	225.183	F(6, 517) = 230.77	$(\delta_{max}/L)^2$	−3.05824	0.743889	−4.11	0	−4.51965	−1.59682
Total	428219.2	523	818.7748	Prob > F = 0	(δ_{max}/L)	24.97149	4.095759	6.1	0	16.92511	33.01787
				R-squared = 0.7281	$(L_{SMA}/L)^2$	48.73263	9.739459	5	0	29.59885	67.86641
				Adj R-squared = 0.725	(L_{SMA}/L)	−63.5142	10.60582	−5.99	0	−84.35	−42.6784
				Root MSE = 15.006	$(A_{SMA}/A_s)^2$	0.299076	0.081117	3.69	0	0.139717	0.458436
					Constant	23.85597	5.454152	4.37	0	13.14094	34.57099

Table 5. Regression model for M_{rt}/M_{org}.

Source	SS	df	MS	Goodness-of-fit	$\ln(M_{rt}/M_{org})$	Coef.	Std. Err.	t	P > t	(95% Conf. Interval)	
Model	90.04619	4	22.51155	Number of obs = 268	(δ_{max}/L)	0.351534	0.062099	5.66	0	0.229259	0.473809
Residual	6.938488	263	0.026382	F(4, 263) = 853.29	$(\delta_{max}/L)^2$	−0.03753	0.011257	−3.33	0.001	−0.0597	−0.01536
Total	96.98468	267	0.363238	Prob > F = 0	$(L_{SMA}/L)^2$	−0.70269	0.031461	−22.34	0	−0.76464	−0.64075
				R-squared = 0.9285	$\ln(A_{SMA}/A_s)$	0.736527	0.014268	51.62	0	0.708432	0.764621
				Adj R-squared = 0.9274	Constant	3.829082	0.076069	50.34	0	3.679301	3.978863
				Root MSE = 0.16243							

Table 6. Regression model for ST_{rt}/ST_{org}.

Source	SS	df	MS	Goodness-of-fit	ST_{rt}/ST_{org}	Coef.	Std. Err.	t	P > t	(95% Conf. Interval)	
Model	216748.4	4	54187.1	Number of obs = 268	(L_{SMA}/L)	−137.331	3.967807	−34.61	0	−145.144	−129.518
Residual	4298.316	263	16.34341	F(4, 263) = 3315.53	$(L_{SMA}/L)^2$	63.86686	3.612979	17.68	0	56.75282	70.98091
Total	221046.7	267	827.8903	Prob > F = 0	(A_{SMA}/A_s)	24.46517	0.766933	31.9	0	22.95506	25.97528
				R-squared = 0.9806	$(A_{SMA}/A_s)^2$	−1.92955	0.136156	−14.17	0	−2.19764	−1.66146
				Adj R-squared = 0.9803	Constant	56.02788	1.221183	45.88	0	53.62334	58.43242
				Root MSE = 4.0427							

Table 7. Regression model for EN_{rt}/EN_{org}.

Source	SS	df	MS	Goodness-of-fit	$\ln(EN_{rt}/EN_{org})$	Coef.	Std. Err.	t	P > t	(95% Conf. Interval)	
Model	585.3854	5	117.0771	Number of obs = 268	(δ_{max}/L)	2.085338	0.238586	8.74	0	1.615549	2.555128
Residual	102.0269	262	0.389415	F(5, 262) = 300.65	$(\delta_{max}/L)^2$	−0.25739	0.043251	−5.95	0	−0.34255	−0.17222
Total	687.4122	267	2.574578	Prob > F = 0	(L_{SMA}/L)	−4.36291	0.612504	−7.12	0	−5.56897	−3.15686
				R-squared = 0.8516	$(L_{SMA}/L)^2$	0.985633	0.557721	1.77	0.078	−0.11255	2.083819
				Adj R-squared = 0.8487	$\ln(A_{SMA}/A_s)$	1.194	0.05482	21.78	0	1.086056	1.301944
				Root MSE = 0.62403	Constant	0.415448	0.316043	1.31	0.19	−0.20686	1.037756

10. Conclusions

Retrofitting RC BCJs using external unbonded SMA bars was investigated. A three-dimensional FE model, using ABAQUS, was first developed and validated using available experimental results. Experimental results included RC BCJs internally reinforced with steel and SMA bars, and RC beams externally retrofitted with unbonded steel or SMA bars. Good agreement between experimental and numerical results was observed.

A retrofitted BCJ was assumed and analyzed using the developed FE model. Obtained results of the retrofitted BCJ were compared to the results of the original BCJ. An increase of 22% in the beam strength was observed. However, residual displacement was only reduced by 17%. This small recovery is attributed to the big difference in the modulus of elasticity between steel and SMA. To increase the amount of recovered displacement at complete unloading, it is proposed to cut the internal steel bars at the face of the column and replace them with the external SMA bars. The analysis was performed again for the retrofitted beam after cutting the internal bars. It was found that the residual displacement at complete unloading was only 2% of the maximum applied displacement.

Since it is a complicated process to model the BCJ in ABAQUS, a simplified model using the SeismoStruct software was then developed to capture the behaviour of RC BCJs externally reinforced with SMA bars. Results of the simplified model were first validated using the results of the ABAQUS model. Then, it was used to carry out an extensive parametric study to investigate the behaviour of RC BCJs retrofitted using external SMA bars. Three parameters were investigated in this study. These parameters are: (i) ratio between the external SMA reinforcement to the internal steel reinforcement (A_{SMA}/A_s); (ii) ratio between the length of the SMA bars and the full length of the beam (L_{SMA}/L), and (iii) applied drift ratio (δ_{max}/L). Four outputs were used in the parametric study to capture the change happening in the behaviour due to varying of the parameters. These outputs are: (δ_r/δ_{max}), (M_{rt}/M_{org}), (ST_{rt}/ST_{org}), and (EN_{rt}/EN_{org}).

Results of the parametric study were then used to perform multiple linear regression analysis. Different models with different transformations of the inputs were developed for the four outputs. Results of the regression analysis were then summarized in the form of simple equations to determine the optimum amount and length of the used SMA bars.

Acknowledgments

The authors are grateful for the financial support provided by the Natural Sciences and Engineering Research Council of Canada (NSERC).

Conflict of interest

The authors declare that they have no known competing financial interests or personal relationships that could have appeared to influence the work reported in this paper.

References

1. Bindhu KR, Jaya KP, Manicka Selvam VK (2008) Seismic resistance of exterior beam-column joints with non-conventional confinement reinforcement detailing. *Struct Eng Mech*30: 733–761.
2. Yurdakul O, Avsar O (2015) Structural repairing of damaged reinforced concrete beam-column assemblies with CFRPs. *Struct Eng Mech* 54: 521–543.
3. Chalioris CE, Bantilas KE (2017) Shear strength of reinforced concrete beam-column joints with crossed inclined bars. *Eng Struct* 140: 241–255.

4. Golias E, Zapris AG, Kytinou VK, et al. (2021) Effectiveness of the novel rehabilitation method of seismically damaged RC joints using C-FRP ropes and comparison with widely applied method using C-FRP sheets—Experimental investigation. *Sustainability* 13: 6454.
5. Golias E, Zapris AG, KytinouVK, et al. (2021) Application of X-shaped CFRP ropes for structural upgrading of reinforced concrete beam-column joints under cyclic loading—Experimental study. *Fibers* 9: 42.
6. Janke L, Czaderski C, Motavalli M, et al. (2005) Applications of shape memory alloys in civil engineering structures—Overview, limits and new ideas. *Mater Struct* 338: 578–592.
7. Alam MS, Youssef MA, Nehdi M (2007) Utilizing shape memory alloys to enhance the performance and safety of civil infrastructure: a review.*Can J Civil Eng* 34: 1075–1086.
8. Abaqus FEA (2021) ABAQUS Analysis user's manual. Available from: http://130.149.89.49:2080/v6.9/index.html.
9. Scott BD, Park R, Priestley MJN (1982) Stress-strain behavior of concrete confined by overlapping hoops at high and low strain rates. *ACI J* 79: 13–27.
10. Stevens NJ (1987) Analytical modeling of reinforced concrete subjected to monotonic and reversed loading [PhD's thesis]. University of Toronto, Toronto.
11. Youssef M, Ghobarah A (1999) Strength deterioration due to bond slip and concrete crushing in modeling of reinforced concrete members. *ACI Struct J* 96: 956–966.
12. Auricchio F, Taylor RL, Lubliner J (1997) Shape memory alloys macromodeling and numerical simulations of the finite strain superelastic behaviour. *Comput Method Appli M* 146: 281–312.
13. Youssef MA, Alam MS, Nehdi M (2008) Experimental investigation on the seismic behaviour of beam-column joints reinforced with superelastic shape memory alloys. *J Earthq Eng* 12: 1205–1222.
14. Saiidi MS, Sadrossadat-Zadeh M, Ayoub C, et al. (2007) Pilot study of behavior of concrete beams reinforced with shape memory alloys. *J Mate Civil Eng* 19: 454–461.
15. SeismoSoft (2021) SeismoStruct—A computer program for static and dynamic nonlinear analysis of structures. Available from: http://www.seismosoft.com.
16. Auricchio F, Sacco E (1997) Superelastic shape-memory-alloy beam model. *J Intel Mat Syst Str* 8: 489–501.
17. Dunlop P, Simon S (2003) Estimating key characteristics of the concrete delivery and placement process using linear regression analysis. *Civil Eng Environ Syst* 20: 273–290.
18. Montgomery DC, Peck EA, Vining GG (2012) *Introduction to Linear Regression Analysis*, 5 Eds., John Wiley & Sons.

AIMS Press